ADVANCED SCIENCE
Open Access

# Supporting Information

for *Adv. Sci.*, DOI 10.1002/advs.202306088

Peptide Nucleic Acid Clamp-Assisted Photothermal Multiplexed Digital PCR for Identifying SARS-CoV-2 Variants of Concern

*Lexiang Zhang, Rokshana Parvin, Siyue Lin, Mingshuo Chen, Ruixuan Zheng, Qihui Fan* and Fangfu Ye**

## Supplementary Information for

# Peptide Nucleic Acid Clamp-assisted Photothermal Multiplexed Digital PCR for Identifying SARS-CoV-2 Variants of Concern

Lexiang Zhang, Rokshana Parvin, Siyue Lin, Mingshuo Chen, Ruixuan Zheng, Qihui Fan*, Fangfu Ye*

Corresponding author: Qihui Fan, Fangfu Ye

Email: fanqh@iphy.ac.cn; fye@iphy.ac.cn

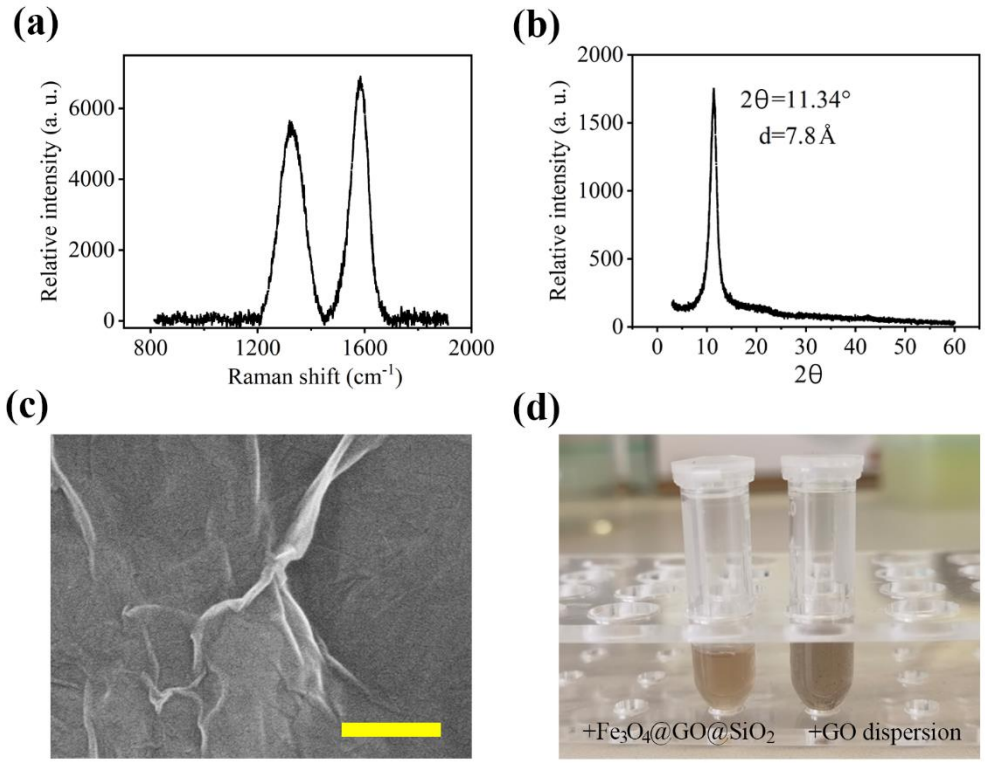


**Figure S1.** Morphology and physicochemical characteristic of GO nanosheets. (a) Raman spectra of graphene oxides showing characteristic peaks centered at ~1350 and 1585 $cm^{-1}$ respectively. (b) XRD analysis. (c) SEM image. (d) Photograph of the dispersion of GO nanosheet and $Fe_3O_4$@GO@$SiO_2$ in 10 % gelatin samples, respectively, after a few rounds of heating to 95 ℃. Scale bar, 250nm in (c).

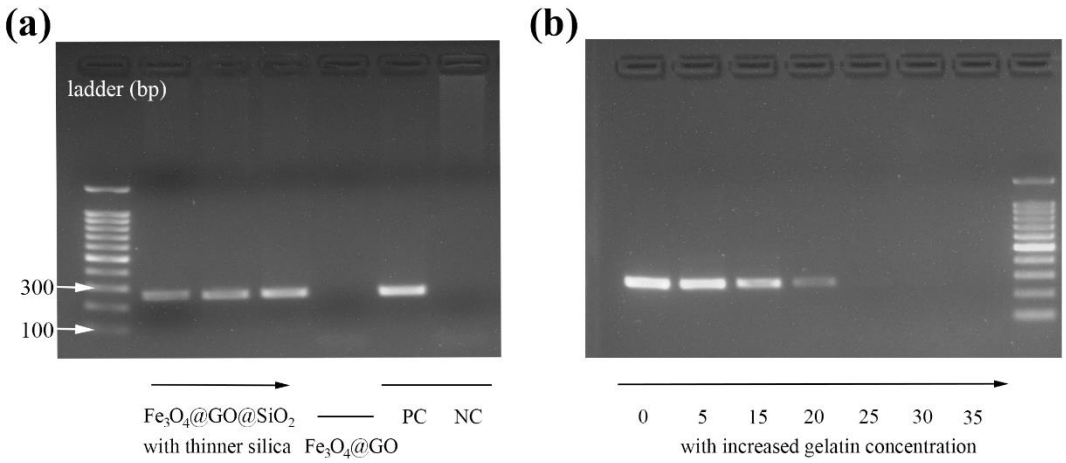


**Figure S2.** Electrophoresis gel images showing biocompatibility of nanocomposite-doped gelatin substrate for PCR. PC and NC columns represent positive and negative controls without nanomaterial addition. PCR efficiency as functions of (a) silica shell thickness and (b) gelatin concentration.

**Table S1.** Size distributions with the polydispersity indexes and standard deviations

| | **diameter** | **polydispersity index** | **standard deviation** |
|---|---|---|---|
| $Fe_3O_4$@GO | 335 | 0.213 | 146.6 |
| $Fe_3O_4$@GO@$SiO_2$ (with four different silica thickness) | 1313 | 0.335 | 365.3 |
| | 1235 | 0.542 | 236.5 |
| | 940 | 0.322 | 312.7 |
| | 742 | 0.314 | 246.9 |

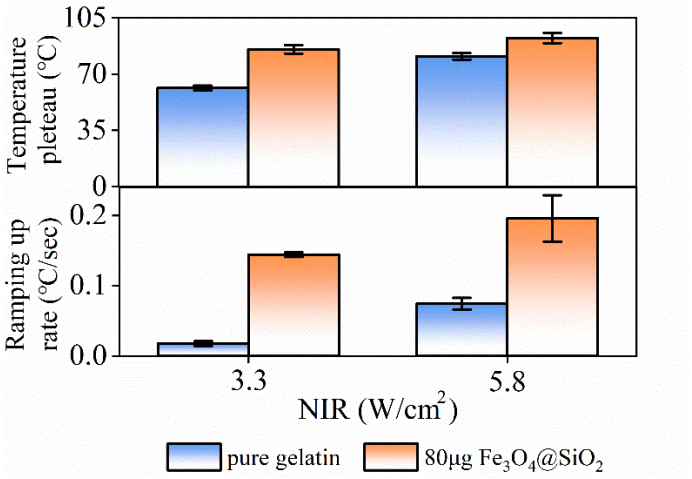


**Figure S3.** Temperature climbing evaluation of 50 μL gelatin samples with and without $Fe_3O_4$@$SiO_2$ NPs addition. Error bar, mean ± s.e.m. (n= 3).

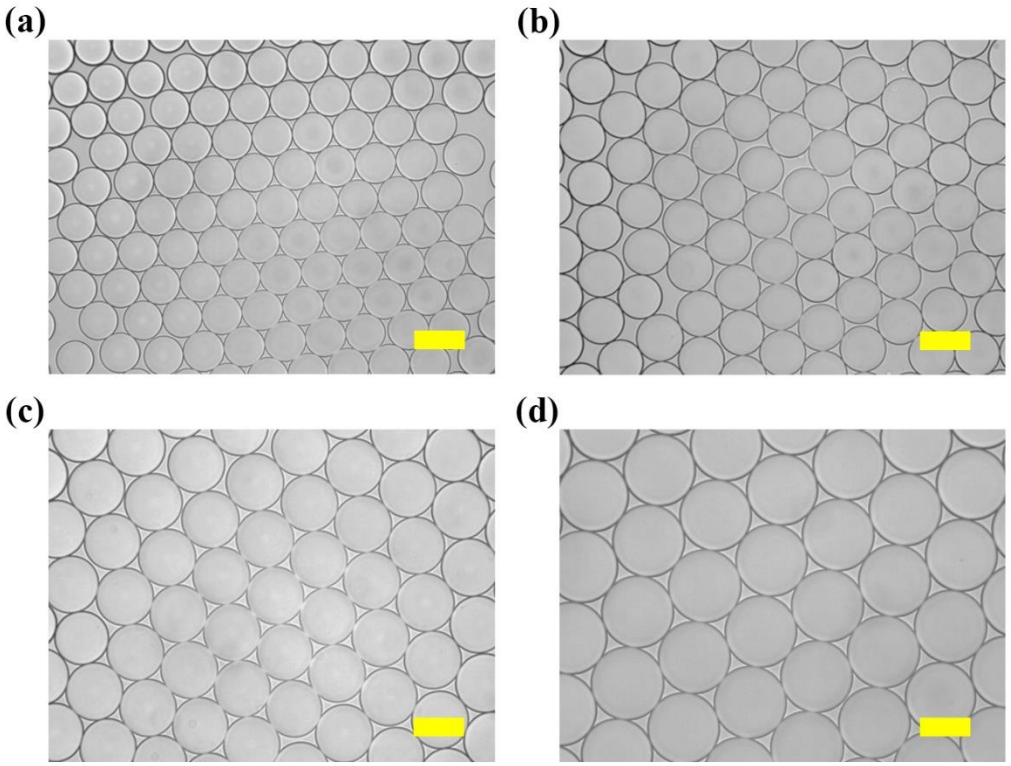


**Figure S4.** Uniformity of produced microcarriers with average diameter of 83, 95, 116, and 126 μm, respectively. Scale bar, 100 μm.

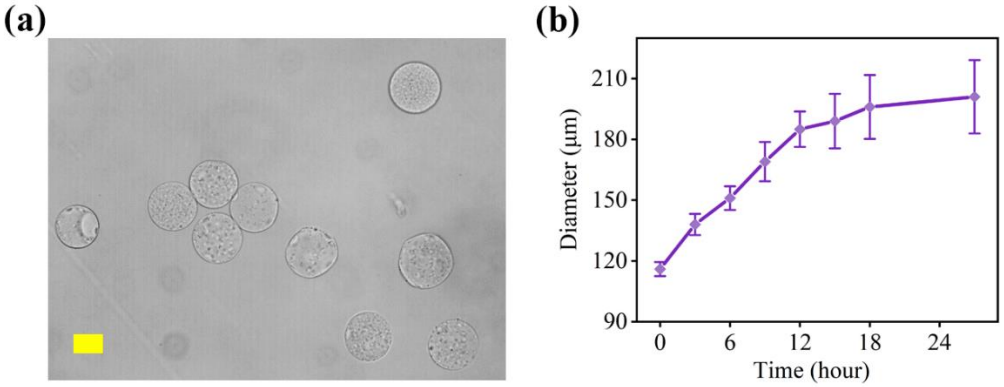


**Figure S5.** Characterization of microcarriers' swelling behavior. (a) Microcarriers with a diameter of 116 μm exhibited a homogeneous size and swelled by 72% over a period of 27 hours. (b) Swelling curves in aqueous solution plotted as a function of time. Scale bar, 100 μm. Error bars, mean ± s.e.m. (n= 3).

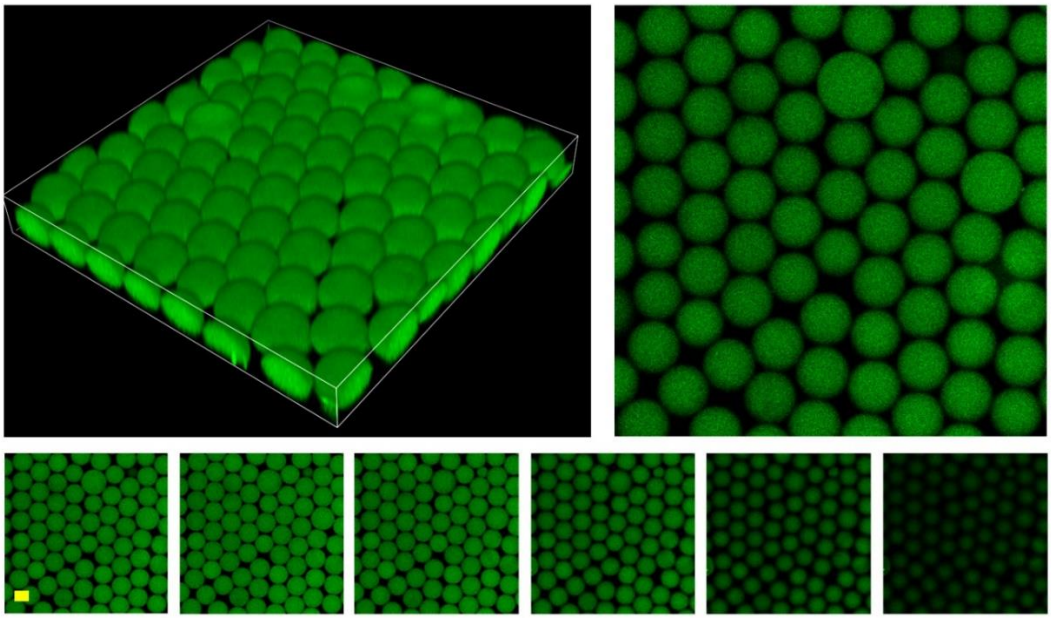

**Figure S6.** A broad field of fluorescence confocal view including a few dozens of microcarriers containing FITC-labelled nanocomposite and a series of slices acquired using the same z-scanning step. Scale bar, 100 μm.

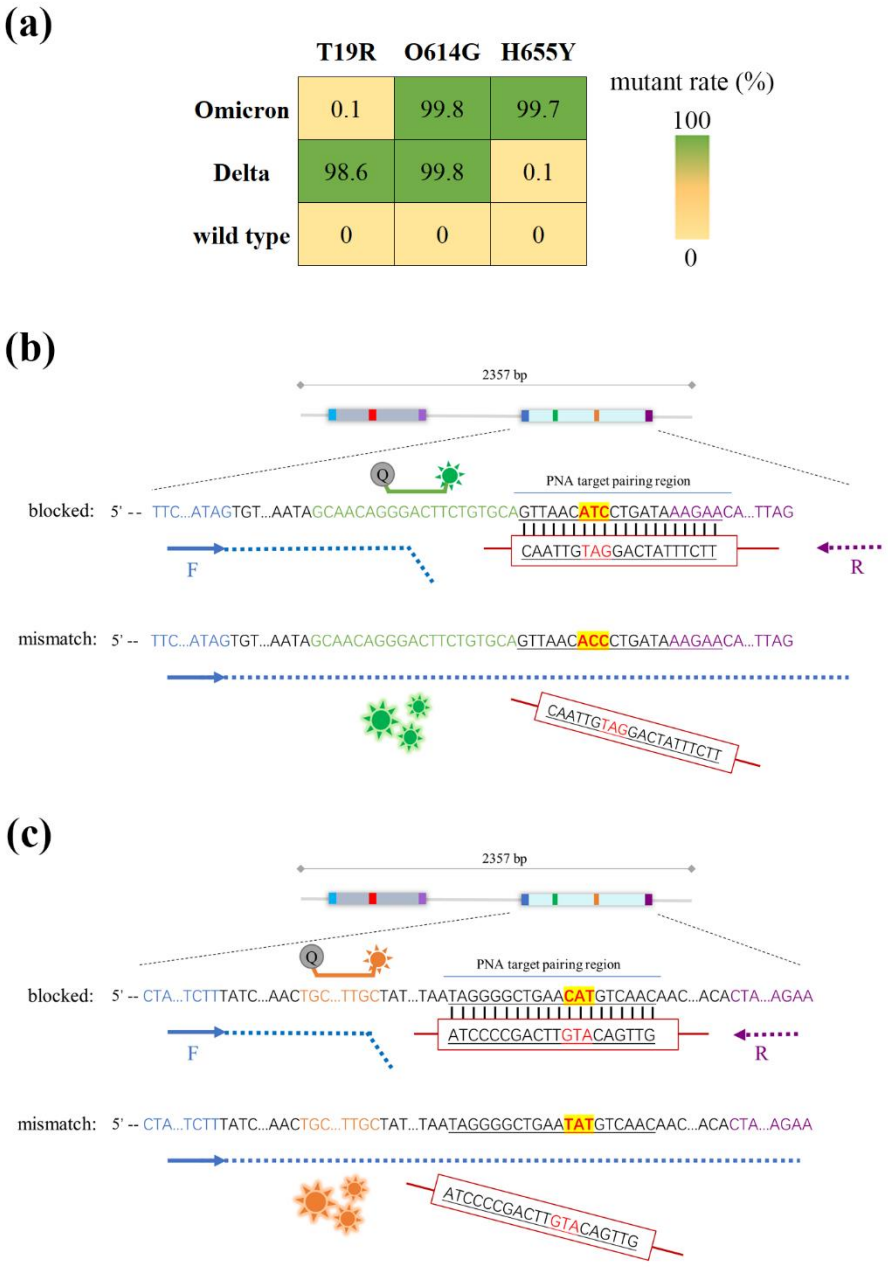


**Figure S7.** (a) Highly conserved SNP signatures used for distinguishing variants of interest based on official reported lineage comparisons. (https://outbreak.info/) Schematic of detecting (b) O614G and (c) H655Y mutations within SARS-CoV-2 spike protein gene. Strategy of designing PNA to selective block wild-type sequence and allow fluorescence signal only derive from targeted mutations. The sequences and positions of the targeted codons, PNA probes, primers, and TaqMan probes are indicated.

**Table S2**. Sequencing of designed PNA clamps, primers and TaqMan probes. 19-2 stands for the second design version targeting at codon 19 of the spike protein gene.

| Name | Sequences (starting from 5') |
|---|---|
| PNA-614 | TTCTTTATCAGGATGTTAAC |
| PNA-19 | TTAATCTTACAACCAGAACT |
| PNA-655 | AGTTGTTGACATGTTCAGCC |
| 19-forward primer | GCCACTAGTCTCTAGTCAG |
| 19-reverse primer | GGTAAGAACAAGTCCTGAG |
| 19-TaqMan (Cy5) | CACACGTGGTGTTTATTACCCTGAC |
| 614-forward primer | CTAACCAGGTTGCTGTTCTT |
| 614-reverse primer | TTCTGCACCAAGTGACATAG |
| 614-TaqMan (FAM) | TGCACAGAAGTCCCTGTTGC |
| 655-forward primer | CTAACCAGGTTGCTGTTCTT |
| 655-reverse primer | TTCTGCACCAAGTGACATAG |
| 655-TaqMan (Cy3) | TGCACAGAAGTCCCTGTTGC |
| PNA-19-v2 | TGTGTTAATCTTACAACCAG |
| PNA-19-v3 | GTTCTGGTTGTAAGATTAAC |
| PNA-19-v4 | TGAGTTCTGGTTGTAAGATT |
| PNA-655-v2 | GTTGACATGTTCAGCCCCTA |
| PNA-655-v3 | CTGAACATGTCAACAACTCA |
| PNA-19-fv | TTCTGGTTGTAAGATTAA |
| PNA-655-fv | TGTTGACATGTTCAGCC |

* v2 and fv represent version 2 of the other available designs and failed version, respectively.

**Table S3.** Significance analysis of different groups in Figures 5b, where "ns" represents not significant.

| fluorescent channel | mutant template % | Cy5 | | | FAM | | | Cy3 | | |
|---|---|---|---|---|---|---|---|---|---|---|
| | | 0.05 | 0.5 | 1 | 0.05 | 0.5 | 1 | 0.05 | 0.5 | 1 |
| Cy5 | 0.05 | | *** | *** | ns | *** | *** | ns | *** | *** |
| | 0.5 | | | *** | *** | ns | *** | *** | ns | *** |
| | 1 | | | | *** | *** | ns | *** | *** | ns |
| FAM | 0.05 | | | | | *** | *** | ns | *** | *** |
| | 0.5 | | | | | | *** | *** | ns | *** |
| | 1 | | | | | | | *** | *** | ns |
| Cy3 | 0.05 | | | | | | | | *** | *** |
| | 0.5 | | | | | | | | | *** |
| | 1 | | | | | | | | | |

**Table S4.** Back-to-back comparison with the bulk qPCR approach based on the assay priming codon 19.

| DNA template input (×$10^4$ copy) | Bulk qPCR (Ct) | | dPCR (bright drop %) | |
|---|---|---|---|---|
| | average | SD. | average | SD. |
| 19.4 | 23.8 | 1.7 | 93.0 | 1.7 |
| 11.6 | 25.5 | 1.6 | 81.7 | 1.2 |
| 5.5 | 26.8 | 0.8 | 58.7 | 3.1 |
| 0.6 | 30.8 | 1.2 | 12.7 | 1.5 |
| 0 (blank) | 32.7 | 1.0 | 0.2 | 0.1 |

* DNA template inputs were deduced from bright drop percentage in dPCR assay.

* The LoD of bulk qPCR was around $5\times10^4$ copy, beyond which the Cq was indistinguishable from the blank control.

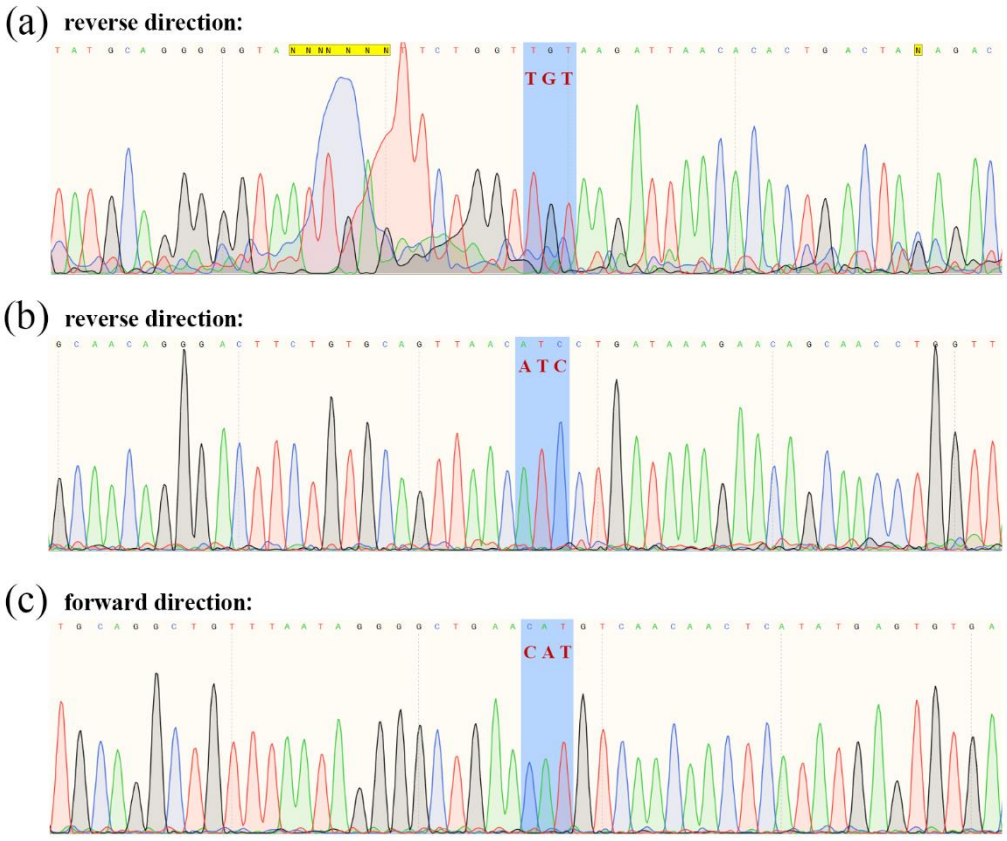


**Figure S8.** Sanger sequencing analysis of the NIR-responsive dPCR products harboring the wild type reads at codon (a) 19, (b) 614 and (c) 655.

**Table S5.** Synthetic plasmid containing the sequence of spike protein gene.